

CENPD-398-NP

**The Advanced PHOENIX and POLCA Codes for
Application to Pressurized Water Reactors**

LEGAL NOTICE

THIS REPORT WAS PREPARED AS AN ACCOUNT OF WORK SPONSORED BY ABB C-E NUCLEAR POWER, INC. NEITHER ABB C-E NUCLEAR POWER, INC. NOR ANY PERSON ACTING ON ITS BEHALF:

A. MAKES ANY WARRANTY OR REPRESENTATION, EXPRESS OR IMPLIED INCLUDING THE WARRANTIES OF FITNESS FOR A PARTICULAR PURPOSE OR MERCHANTABILITY, WITH RESPECT TO THE ACCURACY, COMPLETENESS, OR USEFULNESS OF THE INFORMATION CONTAINED IN THIS REPORT, OR THAT THE USE OF ANY INFORMATION, APPARATUS, METHOD, OR PROCESS DISCLOSED IN THIS REPORT MAT NOT INFRINGE PRIVATELY OWNED RIGHTS; OR

B. ASSUMES ANY LIABILITIES WITH RESPECT TO THE USE OF, OR FOR DAMAGES RESULTING FROM THE USE OF, ANY INFORMATION, APPARATUS, METHOD OR PROCESS DISCLOSED IN THIS REPORT

Copy No. _____

CENPD-398-NP

The Advanced PHOENIX and POLCA Codes for Application to Pressurized Water Reactors

ABB C-E Nuclear Power, Inc.



Copyright 2000, ABB CENP
All rights reserved

This Page Intentionally Left Blank

TABLE OF CONTENTS

1.0 INTRODUCTION	5
1.1 PURPOSE OF THE REPORT	5
1.2 BACKGROUND	6
1.3 APPLICABILITY OF THE REPORT	7
1.4 ORGANIZATION OF THE REPORT	7
2.0 PHOENIX	9
2.1 OVERVIEW OF PHOENIX	9
2.2 PHOENIX CROSS SECTION LIBRARY	9
2.2.1 Processing of ENDF/B-VI Data	9
2.2.2 Resonance Region Treatment	10
2.2.3 Thermal Region Treatment	10
2.3 DEPLETION CALCULATIONS	10
3.0 QUALIFICATION OF THE ENDBF-VI LIBRARY WITH PHOENIX	14
3.1 SUMMARY OF PHOENIX PREDICTIONS	14
3.2 CONCLUSIONS	18
4.0 POLCA	34
4.1 OVERVIEW OF POLCA	34
4.1.1 General Features	34
4.2 CALCULATIONAL FLOW	35
4.3 NEUTRONICS MODEL	36
4.4 CROSS SECTION MODEL	36
4.6 DETECTOR MODEL	38
4.7 ALBEDO MODEL	40
4.8 XENON TRANSIENT MODEL	41
4.9 PIN POWER RECONSTRUCTION MODEL	41
4.9.1 Radial Shape Function	42
4.10 AXIAL HOMOGENIZATION	43
4.11 DEPLETION CALCULATIONS	44
4.11.1 Nuclide Concentration Tracking	44
4.11.2 Detector Depletion	46
4.12 POWER PEAKING FACTORS AND THERMAL MARGINS	47
4.12.1 Power Peaking Factors and Distributions	47
4.12.2 Fission Heat Load Calculations	48
4.12.3 Pellet-Clad Interaction	49
5.0 POLCA QUALIFICATION	51
5.1 NEUTRONIC MODEL VERIFICATION	51
5.1.1 IAEA Benchmark	52
5.1.2 BIBLIS Benchmark	52
5.1.3 DVP Benchmark	53
5.1.4 Intra-Nodal Depletion Benchmark	54
5.2 PIN POWER CALCULATIONAL CAPABILITY QUALIFICATION	55
5.2.1 NEACRP-L336 Benchmark	55
5.3 CORE REACTIVITY AND POWER DISTRIBUTIONS	57
5.3.1 POLCA Reactivity Predictions	57
5.3.2 Axial Offset and Power Peaking Calculations	58
5.3.3 Power Distribution Comparisons	59
6.0 SUMMARY	142
6.1 PHOENIX BENCHMARKS TO TEST THE ENDFB-VI LIBRARY	142

6.2 POLCA QUALIFICATION 143
 6.2.1 Reactivity..... 143
 6.2.2 Power Distributions 144
6.3 OVERALL CONCLUSION 145
7.0 REFERENCES 146

LIST OF FIGURES

FIGURE 1.1: ABB CODE SYSTEM FOR BWR NUCLEAR DESIGN AND ANALYSIS.....	8
FIGURE 3.1: KRITZ BA-75 CORE CONFIGURATIONS WITH ASSEMBLY COORDINATES.....	25
FIGURE 3.2: KRITZ BA-75 CASE 2:1 FISSION RATE DISTRIBUTIONS.....	26
FIGURE 3.3: KRITZ BA-75 CASE 2:3 FISSION RATE DISTRIBUTIONS.....	27
FIGURE 3.4: KRITZ BA-75 CASE 3:1 FISSION RATE DISTRIBUTIONS.....	28
FIGURE 3.5: KRITZ BA-75 CASE 3:2 FISSION RATE DISTRIBUTIONS.....	29
FIGURE 3.6: KRITZ PU EXPERIMENTS CORE CONFIGURATIONS.....	30
FIGURE 3.7: KRITZ PU EXPERIMENTS FUEL PIN CONFIGURATIONS	31
FIGURE 3.8: KRITZ PU CASE 1:1 FISSION RATE DISTRIBUTIONS	32
FIGURE 3.9: KRITZ PU CASE 1:4 FISSION RATE DISTRIBUTIONS	33
FIGURE 4.1: POLCA CALCULATION FLOW DIAGRAM	50
FIGURE 5.1: IAEA 2D BENCHMARK, POLCA vs. ANL-7416.....	66
FIGURE 5.2: BIBLIS 2D BENCHMARK, POLCA vs. LABAN.....	67
FIGURE 5.3: DVP BENCHMARK, POLCA vs PDQ	68
FIGURE 5.4: INTRA-NODAL DEPLETION BENCHMARK, POWER DISTRIBUTION BOC1	69
FIGURE 5.5: UO ₂ /MOX CHECKERBOARD FOR NEACRP-L336 BENCHMARK.....	70
FIGURE 5.6: NEACRP-L336 BENCHMARK POWER COMPARISON (UO ₂ ASSEMBLY).....	71
FIGURE 5.7: NEACRP-L336 BENCHMARK POWER COMPARISON (MOX ASSEMBLY)	72
FIGURE 5.8-5.17: CRITICAL BORON CONCENTRATIONS	77
FIGURE 5.18-5.21: AXIAL OFFSET.....	87
FIGURE 5.22-5.36: CORE AVERAGE AXIAL POWER DISTRIBUTIONS	90
FIGURE 5.37-5.81: POWER DISTRIBUTIONS.....	107

LIST OF TABLES

TABLE 2.1: NEUTRON ENERGY GROUP STRUCTURE FOR THE 34-GROUP LIBRARY	11
TABLE 2.2: NEUTRON ENERGY GROUP STRUCTURE FOR THE 89-GROUP LIBRARY	12
TABLE 2.3: CHARACTERISTICS OF THE 34-GROUP PHOENIX LIBRARY	13
TABLE 3.1: PARAMETER RANGES FOR PIN CELL CRITICALS	20
TABLE 3.2: PIN CELL CRITICALS RESULTS (34-GROUP LIBRARY)	20
TABLE 3.3: PIN CELL CRITICALS RESULTS (89-GROUP LIBRARY)	20
TABLE 3.4: EXPERIMENTAL DATA AND RESULTS FOR PIN CELL CRITICALS	21
TABLE 3.5: TRX AND BAPL EXPERIMENTS RESULTS	23
TABLE 3.6: KRITZ BA-75 EXPERIMENTS RESULTS	23
TABLE 3.7: KRITZ BA-75 EXPERIMENTS	23
TABLE 3.8: KRITZ PU EXPERIMENTS RESULTS	24
TABLE 3.9: ISOTHERMAL TEMPERATURE COEFFICIENT FOR KRITZ PU EXPERIMENTS	24
TABLE 3.10: SUMMARY OF BENCHMARK CRITICAL EXPERIMENTS	24
TABLE 5.1: INTRA-NODAL DEPLETION BENCHMARK RESULTS (CYCLE 1)	61
TABLE 5.2: INTRA-NODAL DEPLETION BENCHMARK RESULTS (CYCLE 2)	61
TABLE 5.3: INTRA-NODAL DEPLETION BENCHMARK CONTROL ROD WORTH (RW)	62
TABLE 5.4: SUMMARY OF RESULTS FOR NEACRP-L336 BENCHMARK	62
TABLE 5.5: SUMMARY OF RESULTS FOR F-DELTA H AND FQ COMPARISONS	63

1.0 INTRODUCTION

The two principal computer programs for Light Water Reactor steady-state nuclear design and analysis used by ABB are PHOENIX and POLCA. The PHOENIX code is a two-dimensional multi-group transport theory code used to calculate the lattice physics constants of LWR fuel assemblies. The POLCA code is a two-group nodal code used for the three-dimensional simulation of the nuclear and thermal-hydraulic conditions in LWR cores. In addition, several auxiliary codes are also utilized in order to facilitate calculations and transfer of data between the aforementioned codes.

This Report has the following purpose:

- To describe the methodology of PHOENIX and POLCA for application to Pressurized Water Reactors (PWRs).

1.1 PURPOSE OF THE REPORT

The purpose of Reference 1, CENPD-390-P (The Advanced PHOENIX and POLCA Codes for Nuclear Design of Boiling Water Reactors) was to present the qualification work that has been performed for a new version of the PHOENIX/POLCA code system and applied it to the nuclear design of Boiling Water Reactors (BWRs). The qualification results in Reference 1 establish the accuracy and uncertainties associated with the PHOENIX/POLCA system when applied to a BWR. Since the calculational models, approximations and methods in the PHOENIX code are the same as those described in Reference 1, review of the PHOENIX calculational methods is not deemed necessary and the calculational model descriptions are not repeated in this report. Qualification results with the 34-group cross section library are provided in Reference 1, as an illustration of the ABB methodology for qualifying a new cross section library. PHOENIX, and the associated nuclear data pre- and post-processing codes support the new cross section library and the POLCA improvements described in Reference 1. This report addresses specific qualification results as they apply to PWR lattices and nuclear cores.

1.2 BACKGROUND

The PHOENIX and POLCA codes were originally submitted for review in licensing topical reports (References 2 and 3). The nuclear methods used by ABB Atom (formerly ASEA Atom) in Sweden were described in these topical reports.

These reports were reviewed and accepted by the U.S. NRC in References 4 and 5. In 1988, ABB Atom continued the licensing of the ABB BWR reload methodology initiated by Westinghouse. The transfer of the licensing effort from Westinghouse to ABB was formally facilitated by ABB resubmitting NRC approved licensing topical reports under the ABB ownership. The NRC acknowledged the transfer of approval in Reference 6. Reference 1 is the licensing topical report describing the nuclear design and analysis programs resubmitted by ABB. As a result of the acquisition of ABB C-E Nuclear Power, Inc. by the parent company of ABB Atom, the U.S. operations of ABB Atom were consolidated within ABB C-E Nuclear Power, Inc. (Reference 7). Quality control, maintenance, and implementation for the complete ABB U.S. reload fuel licensing methodologies resides with ABB C-E Nuclear Power, Inc.

The ABB LWR nuclear design system of codes is presented in Figure 1.1, which outlines the relationship between the individual computer codes. PHOENIX and POLCA are considered the two major codes in the system, whereas the other codes shown in the figure perform various auxiliary functions.

The calculational models, approximations and methods in the PHOENIX code are the same as those described in Reference 1. The POLCA calculational models are the same as those described in Reference 1.

As noted in Figure 1.1, several auxiliary codes are used in conjunction with PHOENIX and POLCA. The codes FOBUS, HEBE and PHULCAN are used to manipulate cross section library data.. These codes are discussed in Reference 1.

1.3 APPLICABILITY OF THE REPORT

The intended scope of the PHOENIX/POLCA computational methods for application in PWR nuclear cores include the following PWR analysis applications:

- Core power distribution monitoring
- In-core detector simulation
- Simulation of normal operation power maneuvers

1.4 ORGANIZATION OF THE REPORT

Chapter 2 summarizes the basic cross section library and depletion calculations used in the PHOENIX code. PHOENIX is used for generation of few-group microscopic and macroscopic, cell and assembly average cross sections needed as input to POLCA. The calculational models, approximations and methods of PHOENIX are the same as previously reviewed by the NRC. The calculational model descriptions are not repeated in detail in this report.

Chapter 3 contains the verification demonstrating that PHOENIX, in conjunction with the ENDFB-VI cross section library, performs its specified tasks. This verification consists of comparisons with local power distributions from multiple critical experiments. Reactivity data from uniform and nonuniform critical experiments are used to demonstrate that the PHOENIX cross section library performs accurately together with the models for constructing multi-group average microscopic cross sections and for computing the neutron flux distributions within pin cells.

Chapter 4 includes a summary of the calculational flow, methods and approximations in the POLCA code described in Reference 1.

Chapter 5 provides verification of POLCA's models in the form of comparisons with numerical benchmarks. It also contains qualification of the PHOENIX/POLCA code system in the form of comparisons with measurements. The chapter concludes by presenting reactivity and other measured parameters for PWRs.

Chapter 6 provides a summary.

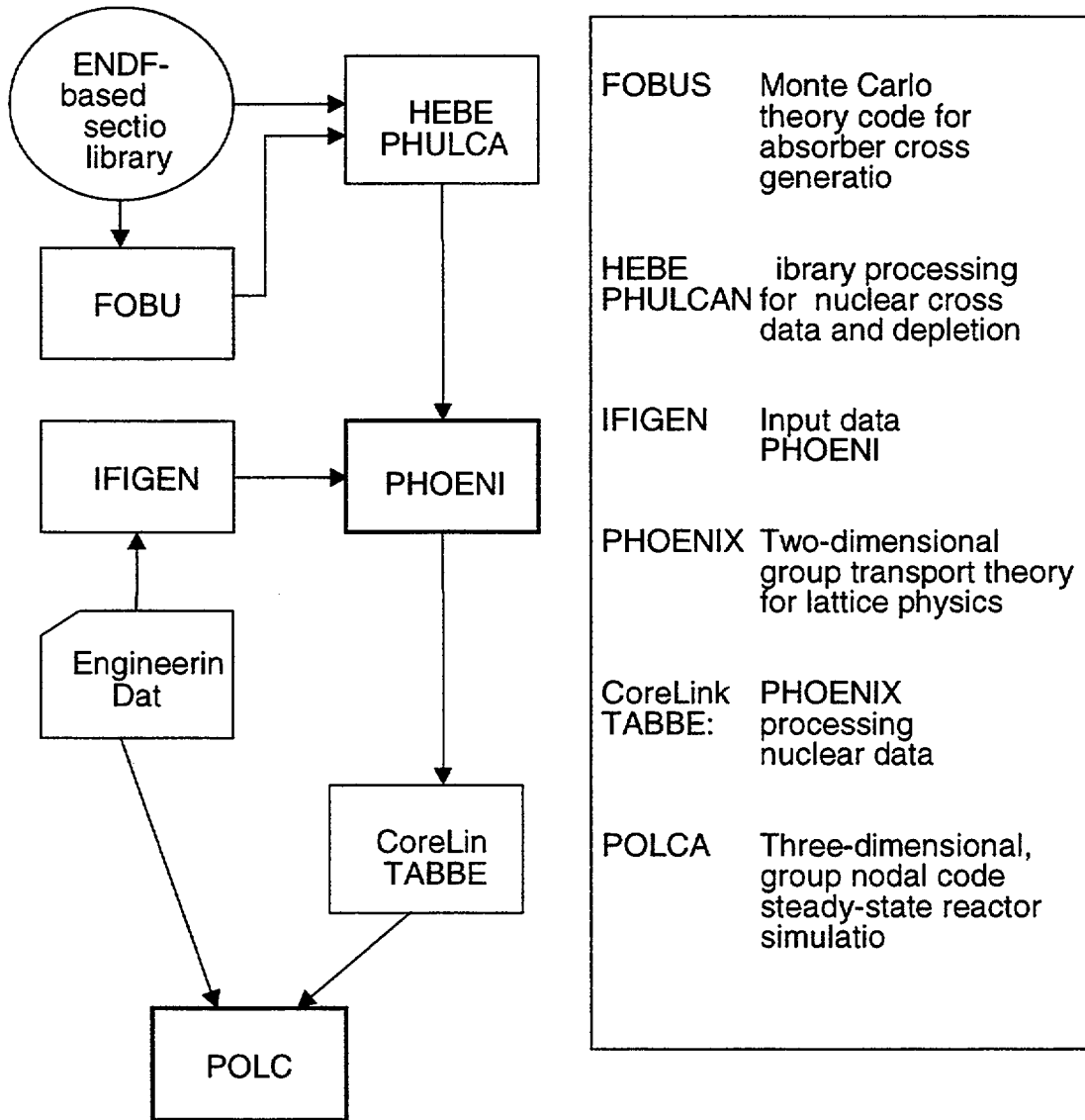


Figure 1.1: ABB Code System for LWR Nuclear Design and Analysis

2.0 PHOENIX

2.1 OVERVIEW OF PHOENIX

The PHOENIX code has been described for BWR use in Reference 1. The applicability of PHOENIX for PWR lattices is also demonstrated in Reference 1. The use of ENDF/B-VI nuclear data in the cross section library used by PHOENIX is also validated in Reference 1. Therefore only a summary of the application to PWRs and the corresponding conclusions are reported in this document.

2.2 PHOENIX CROSS SECTION LIBRARY

The cross section libraries are based on ENDF/B-VI for use with PHOENIX employ 34 and 89 neutron energy groups. They contain multi-group microscopic neutron cross sections, fission spectra, fission product yields, energy yields, and other supplemental data. The qualification of the PHOENIX/POLCA system described in Reference 1 is based on the 34-group library.

2.2.1 Processing of ENDF/B-VI Data

The processing code NJOY 91, with updates through 105 and extended as described below, was used for processing the ENDF/B-VI data. A master library was created and then used for condensation to all other libraries such as the 34-group and 89-group libraries. The group structures of the 34-group and 89-group libraries are shown in Tables 2.1 and 2.2. Table 2.3 lists characteristics of the 34-group library which is used for core design analysis.

The NJOY capabilities were augmented by an extended version of RABBLE. In the extended version used, RABBLE works as a module of NJOY and was capable of reading the continuous cross section data from the PENDF point files of NJOY. This permitted use of more accurate models than the SLBW and a very fine energy mesh in a cylindrical pin.

Appendix A of Reference 1 lists all the materials (MAT): such as isotopes, natural elements, mixtures, burnable absorbers and special materials in the 34-group library. The material identifiers (MAT ID) shown are the identifiers used by PHOENIX. Several burnable absorbers are included which were generated with FOBUS for multiple Gd_2O_3 concentrations and pellet dimensions. The table also shows which materials include resonance tables (RES TABLES) in the library, and which materials only contain absorption cross sections (ABS XS ONLY).

2.2.2 Resonance Region Treatment

Resolved resonances generally fit in the interval 1.855 eV to 9.119 keV, and in this region capture and fission cross sections are in the form of resonance tables. The content of these two-dimensional tables is computed by RABBLE. They are tabulated parametrically in temperature and in equivalent potential scattering via an equivalence theorem. PHOENIX then uses the same equivalence theorem to retrieve and interpolate between values in the table.

2.2.3 Thermal Region Treatment

The ENDF/B-VI files are processed with the THERMR module of NJOY to provide cross sections and scattering matrices in the thermal energy region (0 eV - 3.928 eV). In this region, upscattering is modeled. The cross sections of isotopes containing resonances in the thermal region are Doppler broadened. Scattering matrices are tabulated as a function of temperature, spanning the range of power reactor operation and with sufficient detail to permit linear interpolation.

2.3 DEPLETION CALCULATIONS

Examples of the depletion chains for fission products, heavy elements and for burnable absorbers are shown in Reference 1. These chains may be modified from time to time as new data become available. Any modifications affecting numerical values will be internally documented as part of the process of establishing, validating and documenting the corresponding modified biases and uncertainties.

The method for solving the various chains is similar to the method that was documented in Reference 1. [

]

Table 2.1: Neutron Energy Group Structure for the 34-Group Library

Table 2.2: Neutron Energy Group Structure for the 89-Group Library

Table 2.3: Characteristics of the 34-Group PHOENIX Library

3.0 QUALIFICATION OF THE ENDBF-VI LIBRARY WITH PHOENIX

The primary application of PHOENIX is to generate the few-group nodal cross sections and other physics constants for POLCA. Therefore, the benchmarking of POLCA to plant data described in Chapter 5 provides the best overall qualification of PHOENIX. However, PHOENIX predictions based on the 34-group library have also been directly compared to measured data as summarized below and described in detail in Reference 1.

Comparisons with uniform lattice critical measurements test PHOENIX's ability to accurately calculate reactivity over a wide range of lattice parameters. Because of the simple geometry in those experiments, the comparisons primarily provide verification and validation of the cross section library.

In addition, the ability of PHOENIX to accurately predict bundle reactivity and internal (local) power distributions has been verified using experiments on nonuniform lattices performed at the KRITZ critical facility.

3.1 SUMMARY OF PHOENIX PREDICTIONS

The validation calculations performed with PHOENIX include the following sets of experiments:

The 101 criticals referred to as the "Strawbridge & Barry Criticals," that cover a wide range of lattice parameters, bounding the normal design application for which PHOENIX is intended to be used, and providing a severe test of PHOENIX's ability to accurately predict reactivities over a broad range of conditions.

The TRX and BAPL Criticals, which consist of five experiments with uniform lattices. These criticals are widely used for thermal data testing by the "Cross Section Evaluation Working Group" (CSEWG).

The Nonuniform KRITZ BA-75 Critical Experiments which were performed during 1968-1975 as a series of critical experiments in the KRITZ reactor at Studsvik in Sweden. The KRITZ reactor was designed to perform critical experiments with full size fuel assemblies at temperatures up to 245 °C.

The Nonuniform KRITZ Pu Critical Experiments using mixed oxide fuel rods with 1.50% PuO₂ were performed in 1972-73 in the pressurized KRITZ critical facility in Studsvik, Sweden. These experiments are similar to the KRITZ BA-75 experiments.

Table 3.1 shows that the range of conditions in this experimental data base is extensive and spans the range of modern LWRs.

The results of the comparisons are shown in tables at the end of this chapter.

Table 3.2 shows the average $k_{\text{effective}}$ and corresponding standard error of the mean value (S/\sqrt{N}) for several subgroups of the 101 experiments analyzed. Those results were obtained from PHOENIX using the 34-group library. Table 3.3 shows similar results obtained with the 89-group library. Table 3.4 includes experimental parameters and results (using the 34-group library) for each of the 101 critical experiments.

The results of the reactivity calculations for the 101 pin cell criticals show that PHOENIX agrees well with experiment. Not only is the overall average $k_{\text{effective}}$ of [] satisfactory, but individual category averages are also acceptable. It should also be noted that the mean $k_{\text{effective}}$ and standard errors for the 34-group and 89-group results are in good agreement. This shows that the 34-group, ENDF/B-VI based library performs well.

The results of the TRX and BAPL experiments are shown on Table 3.5.

Table 3.5 presents the PHOENIX results for the five experiments analyzed. For these cases, PHOENIX was used with the 34-group library. The table shows that the BAPL reactivity levels (average $k_{\text{effective}}$ of []) are consistent with the Strawbridge & Barry average for the UO_2 subgroup (average $k_{\text{effective}}$ of []). This again shows good performance for the 34-group library.

However, there appears to be a bias in the TRX cases (average $k_{\text{effective}}$ of []) relative to the Strawbridge & Barry metal lattice subset (average $k_{\text{effective}}$ of []). This may be due to []

The results of these comparisons are shown in Table 3.6 which presents the experimental conditions, measurements and PHOENIX calculated results for each of the twelve cases analyzed. The critical boron concentration, experimental temperature, critical buckling (defined by the water height), water density and calculated $k_{\text{effective}}$ (with PHOENIX) are presented in Table 3.6.

The average $k_{\text{effective}}$ for the twelve configurations analyzed is [] with a standard deviation of []. These results are consistent with the Strawbridge & Barry and the BAPL experiments previously discussed.

The $k_{\text{effective}}$ values for configurations with burnable absorbers are well predicted. Rodded cases are also well predicted. Comparing controlled cases with corresponding uncontrolled cases (2:2 vs. 2:1, 2:4 vs. 2:3), a difference of roughly [] pcm was calculated. This implies a [] of control rod worth, which is considered acceptable.

For cases 2:3, 3:1 and 3:2, measurements were performed both at high and low moderator temperatures. This allows the computation of the isothermal temperature coefficient (ITC) for those cases. The ITC can be obtained by assuming that any soluble boron calculation error is negligible and comparing $k_{\text{effective}}$ values at high and low temperatures for the three pairs of measurements. Table 3.7 shows the computed ITCs.

Although the calculated temperature coefficient is nonzero, the average value of [] represents a major improvement in calculational accuracy relative to calculations performed with earlier cross section libraries. Results using previous libraries have been on the order of []. This progress is due to improvements in U-235 thermal cross sections provided by the ENDF/B-VI data .

Figures 3.2 through 3.5 show the comparisons between the measured and calculated fission rate distributions, which have been normalized to the averaged fission rate density of all measured pins for each experiment. They correspond to case 2:1 at 23.5°C, case 2:3 (with BA) at 243.2°C, case 3:1 at 242.3°C and case 3:2 (with BA) at 241.9°C, respectively.

The agreement between measurement and calculated fission rates is excellent with an average deviation of []. The experimental uncertainty is claimed to be in the order of 1 to 2%. The maximum difference observed was only [].

The configuration for the Non-uniform KRITZ experiments was a square array of 16 fuel assemblies. The assemblies consisted of three different types of 8x8 fuel pins:

- BWR-70 64 UO₂ pins,
- Pu-Island 45 UO₂ pins + 19 PuO₂/UO₂ pins,
- Pu-Max 8 UO₂ pins + 56 PuO₂/UO₂ pins.

The UO₂ pins were enriched to 1.86 wt% U-235. The PuO₂/UO₂ pins were 0.16 wt% U-235/U and 1.50 wt% PuO₂/UO₂. Figure 3.6 shows the KRITZ core arrangements for these experiments, and Figure 3.7 shows the three types of fuel assemblies.

The results are shown in Table 3.8 which presents the experimental conditions, measurements and calculated PHOENIX results for each of the

eight cases analyzed. The critical boron concentration, experimental temperature, critical buckling (defined by the water height), water density and $k_{\text{effective}}$ calculated by PHOENIX are presented in Table 3.8.

The average $k_{\text{effective}}$ for the eight configurations analyzed is [] with a standard deviation of []. No significant difference appears to exist between PuO_2 and UO_2 cases. This absence of a criticality bias between PuO_2 and UO_2 cases is presumably a result of the improved Pu cross section data in ENDF/B-VI. The results are consistent with the Strawbridge & Barry, BAPL and the KRITZ BA-75 cases previously discussed.

The ITCs are computed for two KRITZ PU configurations as was done for the KRITZ BA-75 cases. Table 3.9 shows the computed ITCs. The resulting isothermal temperature coefficient [], which is considered to be acceptable.

Figures 3.8 and 3.9 show the comparison between measured and calculated fission rate distributions for case 1:1 at 241.1°C and case 1:4 at 239.2°C, respectively (for case 1:4, only pins in the central assembly (2,3) were measured.) The results were normalized to the averaged fission rate density of all measured pins for each experiment.

The agreement between measured fission rate distributions and calculated values is excellent with a mean absolute deviation of [], and a maximum difference of []. As for the KRITZ BA-75 experiments, the experimental uncertainty for these experiments is claimed to be on the order of 1 to 2%.

3.2 CONCLUSIONS

The experimental conditions covered by these benchmarks demonstrate the reliability of PHOENIX and its 34-group library over a broad range of conditions.

Table 3.10 provides a summary of the benchmark critical experiment results in this chapter. The relatively high standard deviation observed for the Strawbridge & Barry set seen in Table 3.10 is attributed to the relatively broad range of conditions and the use of measured data from a wide range of sources. The standard deviation in Table 3.10 of [] is not markedly different from that found by Strawbridge & Barry in 1965 while the category means and overall means are significantly different. This indicates that experimental errors may be larger than the errors in modern methods.

The conclusions from each group of comparisons may be summarized as follows:

1. The calculated reactivity level for the overall collection of Strawbridge & Barry criticals (101 cases) and for the various subgroups is in excellent agreement with the measurements (see Table 3.2).
2. The three BAPL cases are the most relevant for LWR application. Both the reactivity level and standard deviation are excellent (see Table 3.5).
3. The KRITZ experiments provide good reactivity benchmarks for the combination of PHOENIX and the 34 cross section library. These cases were complex core geometries with homogeneous and inhomogeneous fuel designs as well as variations in U and Pu and burnable absorber content.

The 12 cases in the KRITZ BA-75 series reflect the capability of PHOENIX and the 34 cross section library to accurately treat reactivity, burnable absorber worth, control rod worth, and relative pin power. They also demonstrate a relatively low reactivity dependence on moderator temperature. Reactivity level is predicted with the same excellent consistency as for the Strawbridge & Barry and BAPL cases (see Table 3.6). Standard deviations are low and consistent with the BAPL experiments. Control rod worths and burnable absorber worths are well predicted. The isothermal temperature coefficient calculation performance is markedly improved with the new cross section library relative to older libraries (see Table 3.7).

The KRITZ PU series (8 cases) reflect the capability of PHOENIX and the 34 cross section library to accurately treat reactivity level and relative pin power in PuO₂ lattices (see Table 3.8). Statistical tests show that the predicted mean PuO₂ $k_{\text{effective}}$ values and corresponding standard

deviations are not significantly different than the corresponding values for UO_2 lattices. This consistency of PHOENIX's predictive capability for UO_2 and PuO_2 experiments represents a significant improvement which is attributed to the new ENDF/B-VI based library. The results confirm the reliability of PHOENIX in the presence of high Pu concentrations and for high inter-assembly leakage.

In overall conclusion, these benchmark calculations reflect the capability of PHOENIX with the new ENDF/B-VI based cross section library to accurately predict reactivity level with very low deviations as well as accurately predict relative pin power (fission rate) distributions. Isothermal temperature coefficient performance, as well as predicted control rod worths and burnable absorber worths, have improved relative to older cross section libraries. The combination of these results confirm that PHOENIX, in conjunction with the new ENDF/B-VI based 34-group library, provides state-of-the-art reactivity and relative pin power predictions for a broad range of conditions and temperatures.

Table 3.1: Parameter Ranges for Pin Cell Criticals

	Experiment	Typical Modern LWR Fuel
Water / U ratio	1.00 - 11.94	2.0 - 5.0*
Lattice pitch (cm)	0.95 - 4.95	1.20 - 1.63
Pellet diameter (cm)	0.44 - 2.35	0.78 - 1.04
Clad outer diam (cm)	0.44 - 2.35	0.95 - 1.25
Enrichment (wt%)	1.04 - 4.07	0.71 - 5.00
Boron content (ppm)	0 - 3392	0 - 3000

* Void and gaps in BWR fuel considered

Table 3.2: Pin Cell Criticals Results (34-Group Library)

Experiment Group	Number of Data Points	Average $k_{\text{effective}}$	Standard Error of Mean Value (pcm)
Hexagonal Lattice	74	[1.00098]	[88]
Square Lattice	27	[1.00058]	[148]
Aluminum Clad	56	[0.99867]	[68]
Stainless Steel Clad	25	[0.99991]	[151]
Dissolved Boron	7	[1.00023]	[106]
No Boron	94	[1.00092]	[81]
UO ₂ Experiments	40	[0.99957]	[115]
Uranium Metal Experiments	61	[1.00173]	[99]
All Data	101	[1.00087]	[75]

Table 3.3: Pin Cell Criticals Results (89-Group Library)

Experiment Group	Number of Data Points	Average $k_{\text{effective}}$	Standard Error of Mean Value (pcm)
Hexagonal Lattice	74	[1.00082]	[83]
Square Lattice	27	[0.99989]	[148]
Aluminum Clad	56	[0.99882]	[69]
Stainless Steel Clad	25	[0.99921]	[148]
Dissolved Boron	7	[0.99949]	[98]
No Boron	94	[1.00065]	[77]
UO ₂ Experiments	40	[0.99896]	[115]
Uranium Metal Experiments	61	[1.00163]	[91]
All Data	101	[1.00057]	[72]

Table 3.4: Experimental Data and Results for Pin Cell Criticals

Table 3.4: Experimental Data and Results for Pin Cell Criticals (Cont'd)

Table 3.5: TRX and BAPL Experiments Results

Experiment	$k_{\text{effective}}$
TRX-1	[0.99403]
TRX-2	[0.99603]
BAPL-1	[0.99880]
BAPL-2	[0.99907]
BAPL-3	[0.99987]

Table 3.6: KRITZ BA-75 Experiments Results

Core No.	Boron Conc.(ppm)	Temp (C)	Buckling (m^{-2})	Water (g/cm^3)	Control Blade	BA pins*	Calc. $k_{\text{effective}}$
2:1	304.6	23.5	7.942	0.9975	no	0	[0.99911]
	364.5	24.2	3.454	0.9973	no	0	[0.99967]
2:2	33.5	22.4	7.555	0.9977	yes	0	[1.00109]
	78.7	23.5	3.895	0.9975	yes	0	[1.00182]
2:3	266.2	23.5	3.979	0.9975	no	2	[0.99981]
	247.4	243.2	3.634	0.8091	no	2	[0.99827]
2:4	33.5	22.5	3.186	0.9975	yes	2	[1.00177]
2:5	52.8	20.6	3.103	0.9982	no	7	[0.99928]
3:1	306.2	22.5	5.580	0.9975	no	0	[0.99901]
	366.2	242.3	2.866	0.8103	no	0	[0.99768]
3:2	31.9	18.9	8.317	0.9985	no	5	[0.99796]
	63.5	241.9	2.810	0.8109	no	5	[0.99867]

* Number of BA pins in each of the four central assemblies

Table 3.7: KRITZ BA-75 Experiments**Isothermal Temperature Coefficient**

Case	Delta T (°C)	Delta k (pcm)	ITC (pcm/°C)
2:3	219.7	[-154]	[-0.70]
3:1	219.8	[-133]	[-0.61]
3:2	223.0	[+71]	[+0.32]
Average ITC			[-0.33]

Table 3.8: KRITZ PU Experiments Results

Core No.	Boron Conc.(ppm)	Temp (C)	Buckling (m ⁻²)	Water (g/cm ³)	Calc. k _{effective}
1:1	44.7	22.8	7.590	0.9977	[0.99946]
	48.3	241.1	4.200	0.8122	[0.99744]
1:2	61.9	18.6	7.080	0.9985	[0.99996]
	61.9	88.4	7.610	0.9662	[0.99914]
1:4	40.7	22.9	10.290	0.9976	[0.99976]
	44.3	239.2	7.310	0.8150	[0.99636]
1:5	40.7	22.4	11.510	0.9977	[0.99936]
	56.1	88.4	11.060	0.9662	[0.99920]

Table 3.9: Isothermal Temperature Coefficient for KRITZ PU Experiments

Case	Delta T (°C)	Delta k (pcm)	ITC (pcm/°C)
1:1	218.3	[-202]	[-0.92]
1:4	216.3	[-340]	[-1.57]
Average ITC			[-1.25]

Table 3.10: Summary of Benchmark Critical Experiments

Experiment Set	No. of Experiments	k _{effective}	Std Dev (pcm)
Strawbridge & Barry (UO ₂ only)	40	[0.99957]	[727]
BAPL	3	[0.99925]	[56]
KRITZ BA-75	12	[0.99951]	[140]
KRITZ PU	8	[0.99884]	[126]
Pooled Data	63	[0.99945]	[582]

(1,4)	(2,4)	(3,4)	(4,4)
(1,3)	(2,3)	(3,3)	(4,3)
(1,2)	(2,2)	(3,2)	(4,2)
(1,1)	(2,1)	(3,1)	(4,1)

For cases 2:1, 2:2, 2:3, 2:4 and 2:5

(1,4)	(2,4)	(3,4)	(4,4)
(1,3)	(2,3)	(3,3)	(4,3)
(1,2)	(2,2)	(3,2)	(4,2)
(1,1)	(2,1)	(3,1)	(4,1)

For cases 3:1 and 3:2

Figure 3.1: KRITZ BA-75 Core Configurations with Assembly Coordinates

Figure 3.2: KRITZ BA-75 Case 2:1 Fission Rate Distributions

Figure 3.3: KRITZ BA-75 Case 2:3 Fission Rate Distributions

Figure 3.4: KRITZ BA-75 Case 3:1 Fission Rate Distributions

Figure 3.5: KRITZ BA-75 Case 3:2 Fission Rate Distributions

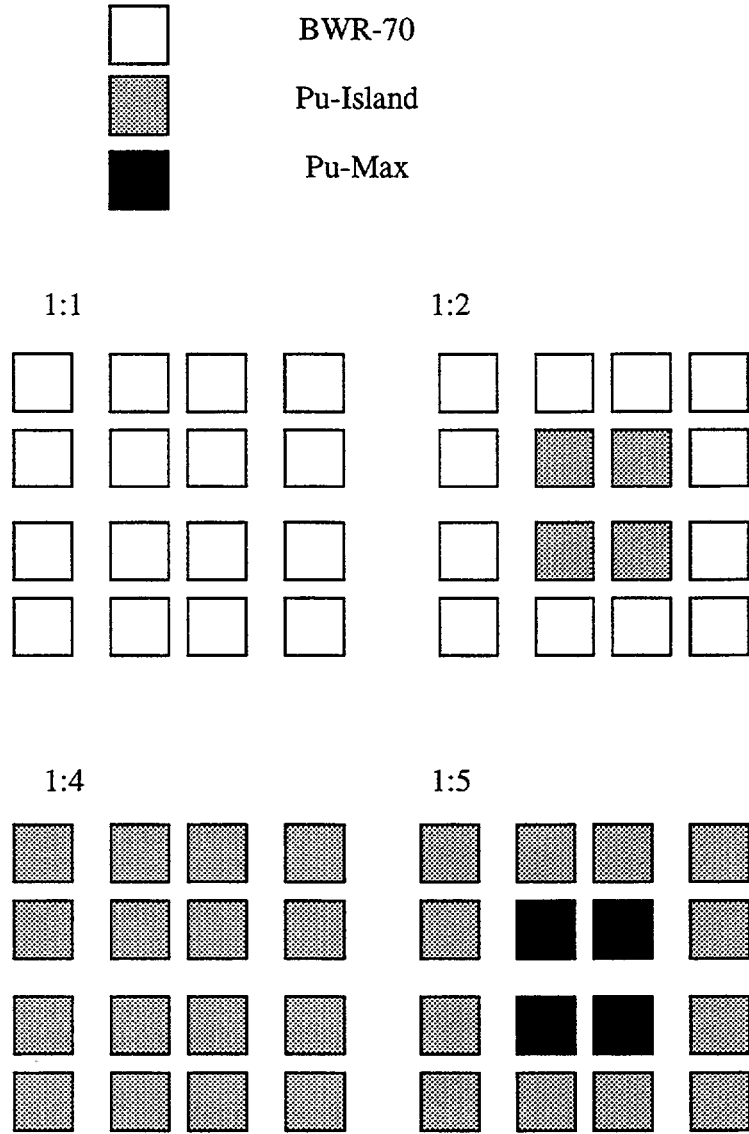


Figure 3.6: KRITZ PU Experiments Core Configurations

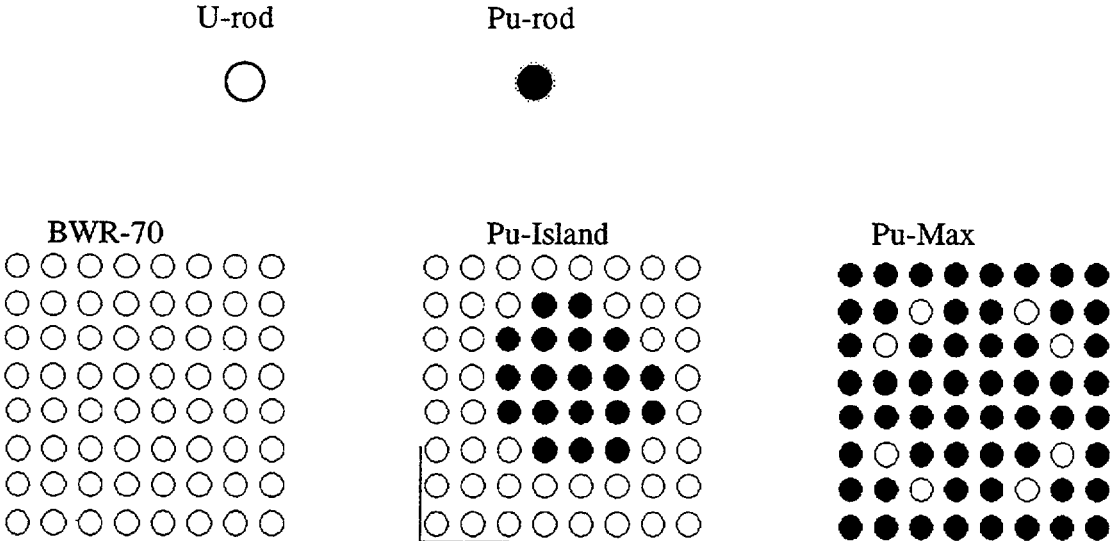


Figure 3.7: KRITZ PU Experiments Fuel Pin Configurations

Figure 3.8: KRITZ PU Case 1:1 Fission Rate Distributions

Figure 3.9: KRITZ PU Case 1:4 Fission Rate Distributions

4.0 POLCA

4.1 OVERVIEW OF POLCA

POLCA is a three-dimensional code for simulating the neutronic, thermal, and hydraulic behavior of a reactor core. The code solves the coupled thermal-hydraulic and neutronic equations. The version described Reference 1 is used for steady-state design and licensing applications as well as for anticipated operational occurrences (AOOs) and accident analyses which can be treated with steady-state methods. The application to PWR calculations takes advantage of the fact that the neutronic, thermal and hydraulic algorithms are the same as those used for BWR calculations.

POLCA solves the two-group diffusion equation employing an analytic nodal method. The code calculates the three-dimensional power distribution in the reactor taking into account all important phenomena that affect the neutronic, thermal and hydraulic behavior of the core. The reactor core is divided into computational nodes in which the neutronic characteristics of each node are described by homogenized equivalent two-group macroscopic cross sections. The three-dimensional power distribution calculated by POLCA includes the thermal-hydraulic feedback effects of the coolant flow, the influence of control rods, the reactivity feedback effects due to Doppler feedback, xenon absorption, soluble boron and coolant density. POLCA can model either quarter-core, half-core, or full core geometries.

4.1.1 General Features

POLCA is the main working tool for in-core fuel management activities. Examples of applications of POLCA are:

- Core reload design
- Control rod worth calculations
- Reactivity coefficient calculations
- Fuel depletion
- In-core instrument analysis (Traveling In-core Probes, Fixed In-core Detectors)
- Load maneuver planning and analysis
- Power increases and decreases between cold conditions and hot full power
- Power distribution control planning
- Boration and deboration analysis
- Core operation optimization

POLCA solves the coupled neutronic and thermal-hydraulic problem with state-of-the-art methods providing a high degree of spatial resolution. The three-dimensional core power distribution can be computed to the local level within each assembly. Distributions of all important parameters required for design and actual licensing applications can also be computed. All core states from cold, xenon free to hot full power are covered.

The geometric flexibility of POLCA includes three main features:

- A. Core radial symmetry may be chosen with:
- No symmetry
 - Half core mirror or rotational symmetry
 - Quarter core mirror or rotational symmetry
- B. The core boundary conditions are represented [].
- C. The computational unit cell used in POLCA's three-dimensional calculations is a segment of a fuel bundle, referred to as a "node". The axial nodalization may be chosen without requirements of equal node heights. The axial mesh structures for detectors and control rods can be chosen independently of the computational mesh used for solving the neutron diffusion equation. Likewise the axial material description of fuel assemblies is independent of the computational mesh.

4.2 CALCULATIONAL FLOW

The structure of POLCA is summarized in Figure 4.1. The code consists of four main parts: input, power/void iteration loop, post-processing, and output. The input and output parts are self explanatory. Most of the calculations are performed in the remaining two parts. The thermal-hydraulics and neutronic equations are solved in the power/void iteration loop. The power/void iteration is bypassed for PWR applications. Pin power reconstruction and thermal margin calculations are performed during post-processing.

4.3 NEUTRONICS MODEL

POLCA solves the two-group diffusion equation employing a method similar to that referred to as the Analytic Nodal Method (ANM). This method takes the three-dimensional diffusion equation and converts it into three one-dimensional equations, with one equation for each spatial direction. The equations are coupled through the neutron leakage from one direction to another, referred to as transverse leakages. The shape of each transverse leakage is estimated by fitting a parabola to the known average leakages of three adjacent nodes. The analytical solution to the inhomogeneous one-dimensional diffusion equation is used to derive a relationship between node surface net currents and node average fluxes. This relationship is then substituted into the node balance equation to eliminate net currents as unknowns to yield an equation which is similar to that resulting from the finite difference approximation. Thus, a very efficient algorithm for solving the diffusion equation is derived with only one unknown per node.

In addition to the use of transverse leakages for spatial decoupling, the second main feature of POLCA's nodal method is a spectral analysis method used to compute the analytic matrix functions which appear in the nodal coupling relations.

Modern homogenization principles are also accounted for in the nodal equations through the use of discontinuity factors to describe flux continuity conditions at nodal interfaces. In addition, smooth intra-nodal variations of cross sections are allowed to account for burnup induced heterogeneities.

The neutronic computational module produces node average fluxes and node interface average fluxes and net currents. The flux variation inside the node is calculated by the pin power reconstruction approach summarized in Section 4.9.

4.4 CROSS SECTION MODEL

The cross section model in POLCA includes a subset of the nuclides in the PHOENIX 34-group library. The choice of nuclides is discussed in Section 4.11. The function of the cross section module of POLCA is to produce:

- Macroscopic two-group, node average cross sections ($D_1, D_2, \Sigma_r, \Sigma_{a1}, \Sigma_{a2}, \nu\Sigma_{f1}, \nu\Sigma_{f2}$)
- Microscopic two-group, node average cross sections
- Two-group discontinuity factors for the four radial sides and four radial edges of a node (f_g 's)
- Number of neutrons emitted per fission (ν), energy release per fission (κ), and iodine and xenon fission yields (γ_i, γ_{Xe})

Each of those variables is obtained by interpolation in cell data tables produced by PHOENIX. Cell data tables contain cross section values as functions of one or more parameters. Each of those parameters represents a physical quantity or phenomenon that influences the few-group cross sections:

- Burnup (E)
- Instantaneous Coolant Density (ρ)
- Coolant Density History (ρ_h)
- Control Rods (CR)
- Spacer Grids (SG)
- Control Blade History (CBH)
- Soluble Boron
- Fuel Temperature
- Xenon
- Heavy-metal and fission product nuclide inventory

The POLCA cross section model typically constructs a given quantity by mathematical representations such as the one illustrated here for macroscopic cross sections:

$$\begin{aligned} \Sigma = & \Sigma^{base}(E, \rho, \rho_h) + \Delta\Sigma^{CR} + \Delta\Sigma^{SG} + \Delta\Sigma^{Bor} \\ & + d_{Dop} \left[\sqrt{T_f} - \sqrt{T_f^{ref}} \right] \\ & + \sum_i \sigma_i \left[N_i - N_i^{ref}(E, \rho_h) \right] + \Delta\Sigma^{SpatialVar} \end{aligned} \quad \text{Eq. 4.1}$$

This cross section model is based on a combination of a “base” cross section and “difference” terms. The base cross sections, Σ^{base} , are computed by PHOENIX at “base conditions”. A base condition is defined as an exposure state (E) with a given instantaneous coolant density (ρ) for a depletion case with a given coolant density history (ρ_h), absence of control rods, no spacer grids, reference fuel temperature (T_f^{ref}) and reference power density (yielding a reference Xenon equilibrium concentration N_{Xe}^{ref}).

The difference terms represent perturbations of the base states with regard to the insertion of control rods ($\Delta\Sigma^{CR}$) or spacer grids ($\Delta\Sigma^{SG}$), or variations of boron concentration ($\Delta\Sigma^{Bor}$) or fuel temperature ($d_{Dop}[\sqrt{T_f} - \sqrt{T_f^{ref}}]$).

Depleting at conditions different from the reference conditions utilized in PHOENIX to generate the cell data results in an isotope inventory (N_i) that differs from that which is obtained at reference conditions. POLCA accounts for this phenomenon by explicitly tracking all important nuclides (i) and corrects for these isotopic deviations through the next-to-last term in Eq. 4.1.

Likewise, burnup induced intra-node effects are accounted for via a spatial variation correction term which is internally computed from isotopic and burnup information on the sides of all nodes ($\Delta\Sigma^{\text{SpatialVar}}$). The spatial variation correction provides variations in spectral history relative to the history built into the base cross sections.

Cell data are normally represented by three dimensional tables with entries for E , ρ_h , and ρ . []

For accurate evaluation of history effects, microscopic cross sections are needed. They are computed using the following equations:

$$\sigma_i = \sigma_i^{\text{base}}(E, \rho) + \Delta\sigma_i \quad \text{Eq. 4.2}$$

$$\Delta\sigma_i = \Delta\sigma_i^{\text{SG}} + \Delta\sigma_i^{\text{CR}} + \Delta\sigma_i^{\text{Bor}} + \Delta\sigma_i^{\text{Dop}} \quad \text{Eq. 4.3}$$

Microscopic cross sections are computed in much the same way as macroscopic cross sections, except that burnup induced effects as well as the nonlinear isotopic spectral effects are not considered to be required. []

4.6 DETECTOR MODEL

The detector module of POLCA handles two types of response simulations for PWR in-core detectors:

- Neutron in-core detectors
- Gamma in-core detectors

The in-core neutron sensitive response calculation is based on computing the reaction rate induced in the detector by impinging neutrons. This is done by combining detector response functions (D_g^{det}) generated by the lattice code with the point fluxes in the detector location (ϕ_g^{det}) computed by POLCA and summing over the energy groups (g):

$$R_{\text{neutron}} = \sum_{g=1}^2 D_g^{\text{det}} \phi_g^{\text{det}} \quad \text{Eq. 4.4}$$

[]

The in-core gamma response is correlated to a weighted sum of the powers of the fuel pins in the bundles surrounding the detector with expressions of the form:

$$R_{\text{gamma}} = \sum_{K=1}^4 X_K \sum_{i=1}^N w_i^K p_i^K \quad \text{Eq. 4.5}$$

where X_K is the gamma detector constant for assembly K , w_i^K is the importance weight for pin i with pin power p_i^K for assembly K . The pin powers, weighting factors, and detector constants are established by a combination of lattice code (e.g., PHOENIX) and POLCA calculations.

[] The total response at the gamma detector is computed by a weighted sum of contributions from different axial levels.

4.7 ALBEDO MODEL

Two-group albedo boundary conditions are utilized on the outer surfaces of the reactor problem. The outer surfaces may be on the edge of the active core, []

The boundary conditions of the three-dimensional core simulator are expressed by means of partial current albedos in two-energy groups:

$$j^{return} = \underline{\underline{a}} j^{out} \tag{Eq. 4.6}$$

where j represents two-group partial currents and $\underline{\underline{a}}$ is the albedo matrix,

$$[\quad] \tag{Eq. 4.7}$$

[] The albedo concept may be utilized to express a number of special boundary conditions:

- Perfectly reflective boundaries are obtained by setting $\underline{\underline{a}} = \underline{\underline{I}}$
- Zero net current boundary conditions are described by $\underline{\underline{a}} = 0$.
- Zero flux boundary conditions are obtained if $\underline{\underline{a}} = -\underline{\underline{I}}$

The reflector region may be described purely by albedos or, []

] []

[]

] []

4.8 XENON TRANSIENT MODEL

For reactor transients on the time scale of hours, Iodine and Xenon are calculated in separate depletion chains. Two calculational capabilities exist in POLCA. These are the equilibrium Xenon feedback and the Xenon short term time stepping options. The latter can be used to obtain non-equilibrium I-135 and Xe-135 distributions, following a short time step and assuming other nuclide concentrations remain constant. Xenon time stepping combined with successive flux calculations is used to calculate Xenon transients over periods of several hours following a change in operating conditions such as power level or rod bank insertion.

[
|
]

4.9 PIN POWER RECONSTRUCTION MODEL

Design and licensing analyses require local rod power distributions to establish the following types of quantities:

- Local peaking factors
- Thermal quantities such as F_q , F_r , Departure from Nucleate Boiling (DNB)
- Detector response

Since POLCA is a coarse mesh method, its primary function is the calculation of nodal powers resulting in dependent variables which are averaged over individual nodes. Calculation of local pin powers with traditional core simulators, such as POLCA has involved combination of the nodal powers calculated with the core simulator with the unperturbed pin powers established with the lattice code. This option continues to be available with the version of POLCA described in this report. In addition, the POLCA version described herein allows correction of local pin powers calculated with the lattice code based on the results of the nodal calculation performed with POLCA. This correction is referred to as pin power reconstruction.

The pin power reconstruction process involves the superposition of heterogeneous information from the lattice code with a smoothly varying homogeneous power distribution determined from POLCA to obtain a composite power distribution on the pellet level. Specifically, the local (i.e., pellet level) power distribution is given by:

$$P(x, y, z) = S_{rad}(x, y) S_{ax}(z) P^{hom}(x, y, z) \quad \text{Eq. 4.8}$$

In Equation 4.8, $S_{rad}(x,y)$ is the radial fine structure shape function (one value per fuel rod at a given axial height) carried over from the lattice code calculation. This function accounts for the heterogeneous nature of relative rod power distribution due to such effects as individual pin enrichments and the local effects of control rods.

The term $S_{ax}(z)$ is the axial fine structure shape function. This factor accounts for axial heterogeneities such as spacers, control rod tips and enrichment and burnable absorber axial variations. The calculation of $S_{ax}(z)$ is performed in POLCA as discussed in Section 4.10.

The last term, $P^{hom}(x,y,z)$, is the “homogeneous” power distribution inside a node obtained by solving the two-group diffusion equation with realistic boundary conditions [

]. It accounts for global, smooth power variations from such effects as the uneven leakage of neutrons from neighboring nodes operating at different powers and by the fact that the assemblies are depleted in a different environment in the reactor than assumed in the lattice code simulation.

Equation 4.8 makes the basic assumption that the radial and axial heterogeneous dependencies are separable.

4.9.1 Radial Shape Function

The radial shape function in Equation 4.8 is not necessarily equal to the pin power solution $P_{LC}^{het}(x,y)$ of the lattice code but is given in general by:

$$\begin{aligned}
 & \left[\right] \qquad \qquad \qquad \text{Eq. 4.9} \\
 & \left[\right. \\
 & \left. \right] \\
 & \left[\right. \qquad \qquad \qquad \left. \right]
 \end{aligned}$$

4.10 AXIAL HOMOGENIZATION

Material variations within the axial nodes can lead to important reaction rate and flux variations which would not be captured by traditional node average fluxes. Spacers, control rod tips, burnable absorber variation, enrichment zoning, and reflector regions at the assembly ends are examples of those material variations.

The nodal cross sections used by POLCA account for the presence of axial heterogeneities through axial homogenization corrections derived from an axial homogenization method included in POLCA. This method also yields axial discontinuity factors which provide neutron balance in the presence of axial material variations within the node and are utilized in the nodal coupling coefficients. The POLCA treatment of the axial variations also provides a smoothly varying axial flux which can be used to correct the axial power distributions with the axial fine structure function discussed in Section 4.9 to accommodate the heterogeneous variations within the node (i.e., $S_{ax}(z)$ in Equation 4.8).

While inhomogeneous radial effects within the nodes require heterogeneous input from the lattice code, inhomogeneous axial variations are treated entirely within POLCA with a sophisticated axial homogenization procedure.

[

]

4.11 DEPLETION CALCULATIONS

POLCA has the capability to track concentrations of important isotopes, as well as burnups from core average to the local level, core resident times (effective full power hours) and moderator density history, in support of design and licensing analysis applications.

The nuclide concentration tracking capability is described in Section 4.11.1. Various burnups (e.g. nodal, rod average, and assembly average) are used, for example, as independent variables for specifying thermal limits. Moderator density history is an independent variable for the determination of macroscopic cross sections

4.11.1 Nuclide Concentration Tracking

The important time dependent nuclide concentrations dealt with in POLCA can be divided into two groups. The first group contains the Iodine and Xenon depletion chains and involves time constants in terms of hours. Calculation of time dependent Iodine and Xenon concentrations is addressed in Section 4.8. The second group involves isotopes whose buildup and decay is described with time constants at least as large as days. This section deals with isotopes which are in the second group.

The most important heavy nuclides and fission products are tracked explicitly in POLCA. The processes in the mathematical model for the transmutation of nuclides include both production and destruction mechanisms.

For example, nuclide i can be assumed to be produced through a combination of three mechanisms

- direct fission (fission yield γ_i)
- β -decay of its predecessor $i-1$ (decay constant λ_{i-1})
- conversion (microscopic capture cross section $\sigma_{c,i-1}$)

Nuclide i can be assumed to be removed from the system through

- β -decay (decay constant λ_i)
- neutron absorption (microscopic capture cross section σ_c)

Assuming a two neutron energy group model, the depletion process can be described by the number density equation:

$$\begin{aligned}
 \frac{dB_i}{dt} = & \gamma_i (\Sigma_{f1}\phi_1 + \Sigma_{f2}\phi_2) + \lambda_{i-1}A_{i-1} \\
 & + (\sigma_{c1,i-1}\phi_1 + \sigma_{c2,i-1}\phi_2)B_{i-1} \\
 & - \lambda_i B_i - (\sigma_{a1,i}\phi_1 + \sigma_{a2,i}\phi_2)B_i
 \end{aligned}
 \tag{Eq. 4.10}$$

[

]

The isotopes currently selected for explicit representation in POLCA are shown in Appendices B and C of Reference 1. These isotopes are a subset of the set of isotopes provided in the PHOENIX library. The isotopes which are not explicitly treated in POLCA are accounted for in macroscopic cross sections input to POLCA. The macroscopic cross sections input to POLCA are described in Section 4.4.

Examples of the criteria used for selecting nuclides for explicit representation in POLCA are:

- [
-
-
-
-
-]

[]

4.11.2 Detector Depletion

POLCA tracks the depletion of fission chamber type neutron detectors. The active fissionable material in these detectors consists of U-235. Such detectors may be enriched in U-234 to prolong the effective lifetime of the detector through U-235 breeding. The depletion state of a detector accordingly can be represented by the following:

$$\begin{array}{l}
 \left[\begin{array}{l} - \quad [\\ - \\ - \quad] \end{array} \right. \\
 \\
 \left[\right. \\
 \\
 \left. \right]
 \end{array}$$

4.12 POWER PEAKING FACTORS AND THERMAL MARGINS

POLCA edits power peaking factors and distributions as well as parameters used to monitor margins to thermal limits. These parameters can be divided into three categories:

1. Assembly, nodal, and local power peaking factors and power distributions are edited by POLCA to assist in the design process and to support a thorough understanding of the core behavior. These quantities are calculated in POLCA from the power distributions calculated by POLCA as well as those predicted by the lattice code. Power distributions calculated in POLCA are also used in the evaluation of thermal margins.
2. Fission heat load quantities used for monitoring margins to licensing analysis limits are calculated by POLCA. These parameters include quantities such as Linear Heat Generation Rate (LHGR) and Average Planar Linear Heat Generation Rate (APLHGR).
3. Parameters which are used to implement guidelines recommended to protect against Pellet-Clad Interaction (PCI) are input to POLCA. These parameters include specification of PCI thresholds as well as ramp rate and conditioning restrictions. Utilizing these parameters, POLCA calculates conditioning and deconditioning profiles which can be used in the design phase to predict the impact of the PCI guidelines on core operation.

4.12.1 Power Peaking Factors and Distributions

The POLCA calculational methods described in Sections 4.1 through 4.11 provide power distributions from assembly to pin level. These power distributions can be studied directly in the design phase, used to establish a variety of peaking factors which reflect the behavior of the core, or used to establish parameters such as LHR and DNB upon which PWR thermal limits are typically based. A broad editing capability allows consideration of all power distributions required by the analyst from the assembly level to the pin level.

In addition, a broad range of quantities which indicate the characteristics of power distributions are available. The following are examples of these parameters:

- Relative nodal power density
- Core power axial offset
- Relative pellet peaking factor within a node
- Relative pin peaking factor within an assembly

- Maximum pin peaking factor within a node
- Maximum relative power density of any node in the core
- Maximum relative power density of any assembly in the core
- Maximum relative power in average axial power profile

4.12.2 Fission Heat Load Calculations

Fission heat load parameters are typically used to establish thermal margins and are derived directly from power distributions.

The Linear Heat Rate (LHGR) for a node is defined as the maximum pellet power transferred from the fuel to the coolant per unit length. LHGR is a measure of the fission heat load of a fuel pin. LHGR is one of the parameters typically used to assure that fuel rod thermal-mechanical design criteria are satisfied.

The LHGR is calculated in POLCA as follows:

$$LHGR = Q_{rel} * P * F_{xyz} * \pi_v * h_x^2 * (1 - \gamma) / N_f \quad \text{Eq. 4.11}$$

where

Q_{rel}	=	Relative core thermal power
P	=	Node power density relative to the entire core
F_{xyz}	=	Pellet power peaking factor relative to all the pellets in the node. []
π_v	=	Nominal volumetric core power density (W/m ³)
h_x	=	Nodal width
γ	=	Fraction of fission power deposited outside the fuel pin via gamma and neutron radiation
N_f	=	Number of fuel pins in node

Ratios of LHGR to the LHGR limit typically based on thermal-mechanical design criteria are calculated and edited to allow monitoring of margin to the thermal limit.

The Average Planar Linear Heat Generation Rate (APLHGR) for a node is defined as the heat conducted from the fuel to the coolant averaged over the fuel rods in the node at the elevation in the node at which the APLHGR is a maximum:

$$APLHGR = Q_{rel} * P * F_z * \pi_v * h_x^2 * (1 - \gamma) / N_f \quad \text{Eq. 4.12}$$

where the quantities common to Equation 4.11 and 4.12 have the same meaning, and

F_z = Power axial peaking factor in the node relative to the nodal power

Ratios of APLHGR to the APLHGR limit which typically assures that acceptance criteria for postulated Loss of Coolant Accidents are satisfied are edited to allow monitoring of margin to the thermal limit.

4.12.3 Pellet-Clad Interaction

Pellet-clad interaction (PCI) surveillance is performed by monitoring the conditioning and deconditioning of the fuel to allow a given LHGR. A check is performed to determine whether the actual LHGR exceeds the level to which the fuel has been conditioned. PCI tracking is done for any number of user specified fuel pins in each assembly.

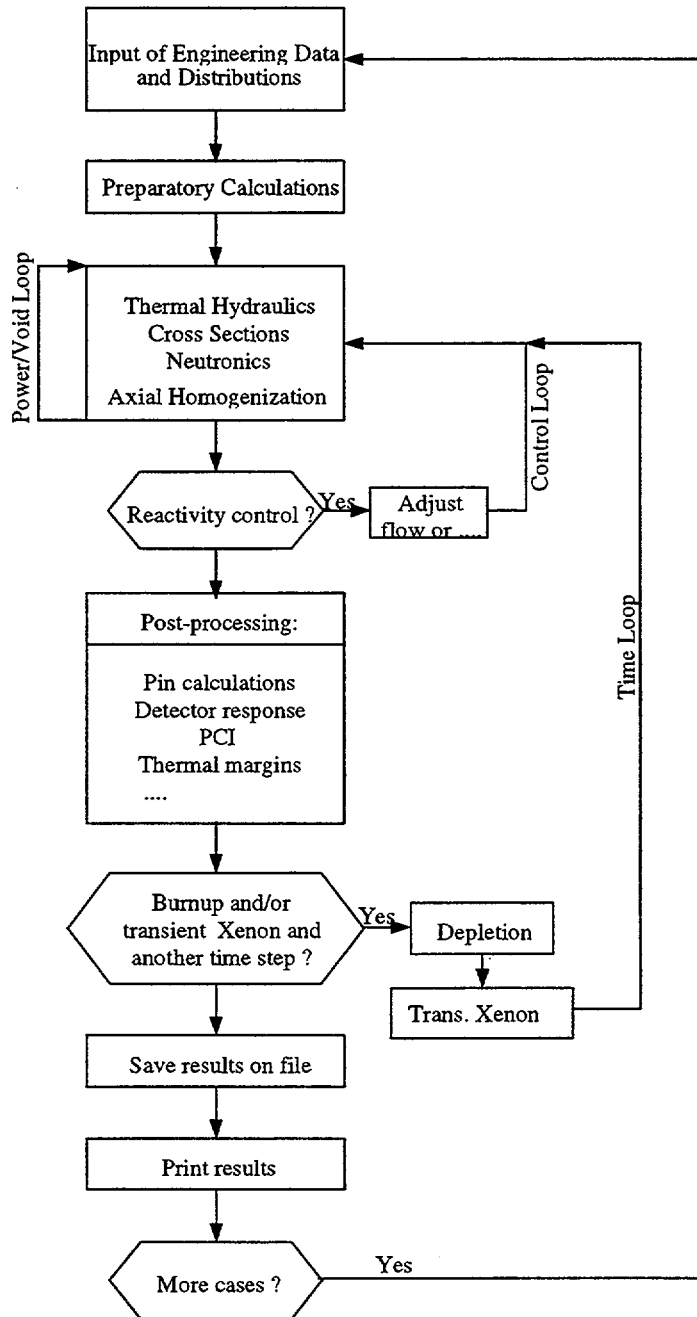


Figure 4.1: POLCA Calculation Flow Diagram

5.0 POLCA QUALIFICATION

The qualification of POLCA is divided into two categories referred to as verification and validation. In the context of this report, verification involves the testing of individual models or combinations of models to verify that they perform as intended. Validation involves the comparison of POLCA predictions with measured data to establish the accuracy of the system operating as a whole.

The POLCA verification is performed by comparison with computational benchmarks generated by means of reference calculations as well as by comparison with experimental data suitable for evaluating the individual model being verified. Specifically, the POLCA verification effort covers the three areas listed below:

- The neutronics model is verified by comparison with established two-dimensional analytical benchmarks. Three of the analytical benchmarks involve power calculations without depletion for both PWR and BWR cores. The fourth benchmark provides verification of the POLCA depletion models.
- The POLCA pin power reconstruction model is verified by comparison with a pin power distribution benchmark.

The POLCA validation involves the evaluation of core follow predictions for PWR reactors. Specifically, reactivity rundown, detector responses calculated by POLCA are evaluated, and compared with the comparable measured parameters.

5.1 NEUTRONIC MODEL VERIFICATION

Comparisons of the POLCA neutronic model calculations with reference solution results for four benchmark problems are discussed in this section. The analytical nodal method in POLCA is extensively tested by each of these benchmarks.

5.1.1 IAEA Benchmark

The International Atomic Energy Agency (IAEA) two-dimensional benchmark problem specified in Reference 8 was evaluated with POLCA. The identifier in Reference 8 for this problem is 11-A2. This benchmark consists of two different fuel bundle types with reflector bundles on the edges of the core and a total of 177 assemblies. The configuration is one-eighth core symmetric. Each assembly has a width of 20 cm and a height of 340 cm. The fuel and reflector bundles have no internal pin structure, and are represented by uniform two-group cross sections. The large flux gradients in the vicinity of the reflector and near the control rods provide a very good test for a code such as POLCA.

The relative assembly powers and $k_{\text{effective}}$ predicted by POLCA were compared with a benchmark reference solution for this configuration. In the discussion below, the term "error" refers to the magnitude of the difference between the relative assembly power predicted by POLCA (P) and the relative assembly power predicted by the reference solution (P_{ref}).

The POLCA solution for this benchmark was compared with Solution 3 (i.e., 11-A2-3) in Reference 8. This solution utilized a nodal method referred to as the nodal expansion method which was run on a very refined spatial mesh (36 meshes per assembly) and should provide a very accurate solution to this problem.

The results obtained with POLCA are compared with those predicted by solution 11-A2-3 in Figure 5.1. Relative to solution 11-A2-3, the POLCA solution has [

]

The conclusion from the two-dimensional IAEA benchmark is that the two computations (POLCA and Solution 11-A2-3 in Reference 8) yield virtually identical results. The small differences observed are characteristic of expected numerical deviations. Overall, this benchmark comparison is a strong indication that the analytical nodal method has been correctly implemented in POLCA and is performing as intended.

5.1.2 BIBLIS Benchmark

As discussed in Reference 9, the BIBLIS benchmark is a two-dimensional model of an operating PWR core with a multi-zone, checkerboard loading. This configuration is one-eighth core symmetric with seven different homogenized fuel compositions and a homogenized reflector. Each assembly has a width of 23.1 cm. The realistic nature of this problem makes it a good test for the POLCA neutronics model which will provide errors or uncertainties similar to those expected in practice.

The POLCA solution was compared with a reference solution generated with the code LABAN as reported in Reference 9. The results obtained with POLCA are compared with those predicted by LABAN in Figure 5.2. Relative to this benchmark, the POLCA solution has [

]

The agreement between the results from POLCA and LABAN are considered to be very good recognizing the realistic nature of the configuration. Therefore, this benchmark comparison corroborates the correct implementation of the analytical nodal method in POLCA and demonstrates that the model is performing as intended.

5.1.3 DVP Benchmark

The DVP problem described in Reference 10 is a two-dimensional BWR case that includes assembly discontinuity factors (ADFs). It is included in this section to demonstrate the ability of POLCA to use ADFs. The core contains three different fuel bundle types with reflector assemblies described as a fourth material. Each assembly has a width of 15.3 cm. The problem is analyzed with zero flux boundary conditions on the outer edge of the reflector. This benchmark was originally defined with multiple reflector layers. For the POLCA evaluation, the problem was modeled with only one reflector layer.

Since the objective of this calculation is to test the implementation and use of ADFs in POLCA, the results calculated with POLCA were compared with the results calculated with an independent advanced nodal method code which also uses ADFs. Accordingly, the MGRAC code described in Reference 11 was used to provide the reference results for comparison with the POLCA results.

The maximum difference in relative assembly powers predicted by POLCA and MGRAC was []. The standard deviation in the relative difference in assembly relative powers was []. The two codes predict a difference in $k_{\text{effective}}$ of []. The very small differences confirm that the implementation and use of ADFs is the same in both codes. Therefore, they confirm the correct application of ADFs in POLCA.

Reference 10 also provides a fine mesh reference solution in the form of a two-group, PDQ calculation which explicitly modeled all fuel pins, water gaps, control blades and the reflector. PDQ is a diffusion theory code with a very fine mesh capability which provides a finite difference solution to the diffusion equation. Comparison of the POLCA results for this benchmark with the PDQ results provides an additional test of the overall performance of the POLCA analytical nodal method with ADFs.

Figure 5.3 shows the differences between the relative assembly powers predicted by POLCA and PDQ. The differences shown in Figure 5.3 are similar to those between PDQ and other state-of-the-art analytical nodal method applications as discussed in Reference 10. Therefore, the comparison in Figure 5.3 further confirms that the analytical nodal method model has been properly implemented in POLCA and is performing as intended.

5.1.4 Intra-Nodal Depletion Benchmark

This benchmark is a two-dimensional, two-group, two cycle depletion test case with octant symmetry. It differs from the other computational benchmarks in that it is a test of the coarse mesh modeling of core depletion as well as the computation of the intra-nodal spatial burnup distribution. This benchmark is described in Reference 12 and the identifier given to this problem there is Case 19.

One third of the core is reloaded at the beginning of the second cycle. Control rods are fully withdrawn during depletion, and the reactor is maintained critical with soluble boron. The length of each cycle is determined by requiring the critical boron at end-of-cycle (EOC) to be zero.

The reference solution to which POLCA is compared in this case is Solution 19-A1-1 in Reference 12. As discussed in Reference 12, this reference solution was obtained by solving the two-group diffusion equation with the nodal expansion method (NEM) with fourth order polynomials and a quadratic transverse leakage approximation. Each assembly was modeled as a 5x5 nodal array in the radial direction in the reference solution. Therefore, this reference solution is judged to provide a sufficiently rigorous flux solution and sufficient intra-nodal detail to provide a good benchmark for POLCA.

In order to capture sufficient intra-assembly detail for meaningful comparison with the reference case, each assembly was described as a 2x2 nodal array radially in POLCA. This option is available in POLCA for PWR applications. Tables 5.1 and 5.2 provide statistics reflecting the relative differences in nodal powers predicted by POLCA and those predicted by the reference case as well as the difference in the prediction of critical boron concentration for the control rods inserted and withdrawn. Rod worth (RW) comparisons are provided in Table 5.3.

The quarter core relative power distribution predicted by the reference solution and the difference in relative power between the POLCA prediction and the reference solution corresponding to the case presented in Table 5.1 (Cycle 1, rods out) are shown in Figure 5.4.

As shown in Tables 5.1 and 5.2 and Figure 5.4, the relative powers and reactivity levels predicted by POLCA are in good agreement with those predicted by the reference solution. The slightly better agreement in the case with control rods withdrawn is consistent with the steeper flux gradients caused by the insertion of control rods. Table 5.3 shows that control rod worths predicted by POLCA are also in good agreement with those predicted by the reference solution. Therefore, the comparisons between the POLCA and reference solution for this benchmark provide confirmation that the advanced nodal method and the POLCA depletion models have been correctly installed in POLCA and are performing as intended.

5.2 PIN POWER CALCULATIONAL CAPABILITY QUALIFICATION

The capability of the pin power reconstruction model in POLCA to accurately predict pin powers is demonstrated in this section by comparisons of POLCA predictions with the results of a higher order reference solution for a hypothetical 17x17 PWR core. In addition, the overall capability of POLCA to predict fuel pin powers in operating BWR cores is confirmed by comparisons of POLCA predictions with fuel rod gamma scan measurements performed at two European reactors.

5.2.1 NEACRP-L336 Benchmark

This section contains POLCA predictions of pin powers for the C3 configuration in the collection of NEACRP-L336 benchmarks described in Reference 13.

The C3 NEACRP-L336 benchmark is an infinite checkerboard core consisting of 2x2 arrays of unrodded UO₂ and MOX 17x17 assemblies. This configuration is shown in Figure 5.5. This benchmark can be used to test the pin power reconstruction capabilities of modern nodal codes.

The reference results to which the POLCA predictions were compared were calculated with the MGRAC code discussed in Reference 11. The MGRAC code is a multi-dimensional diffusion code with fine mesh capability. MGRAC also has the capability to generate the equivalent node-average quantities required by POLCA. Utilization of these equivalent nodal quantities in POLCA and subsequent comparison with the MGRAC fine mesh solution isolates the pin power capability of POLCA and allows a specific test of that capability without contamination by depletion and thermal-hydraulic feedback effects.

The reference results were generated by means of heterogeneous calculations in which each pin cell was explicitly modeled using an analytic nodal model and a mesh structure corresponding to 4 mesh points per pin cell. Auxiliary calculations with 25 mesh points per pin cell yielded differences of about [] in $k_{\text{effective}}$ and [] in pin powers indicating that the mesh structure used is

sufficient to yield an accurate, spatially converged diffusion theory reference solution.

The POLCA model described each assembly as four nodes in a 2x2 array. Sensitivity calculations with a single node per assembly demonstrated that the two nodalization schemes did not yield markedly different results for realistic conditions.

Figures 5.6 and 5.7 provide detailed comparisons of the reference solution and POLCA results for the UO₂ and MOX assemblies, respectively. Each square in Figures 5.6 and 5.7 represents a location in the 17x17 array. The shaded non-central locations are control finger guide tubes, while the central shaded location is an instrument guide tube. The reference pin power, the predicted POLCA pin power, and the difference in the powers predicted by POLCA and the reference solution are listed in each of the fuel rod locations. Table 5.4 summarizes the results. Pin powers are normalized to an average of 1.0 for all fuel rods in the assembly array shown in Figure 5.8.

The comparisons in Figures 5.6 and 5.7 and Table 5.4 indicate that the POLCA pin power reconstruction models are providing accurate results and are performing as expected.

5.3 CORE REACTIVITY AND POWER DISTRIBUTIONS

Further qualification of the POLCA capability to predict reactivity levels and power distributions is provided in the section. POLCA simulations of operating plant depletions and comparisons of POLCA predictions with measurements for one PWR over several cycles of operation are presented.

The ability to predict core reactivity, hence the depletion characteristics of an operating core, is demonstrated by comparisons of the critical soluble boron rundown measured at the plant and predicted by POLCA. POLCA calculates the critical soluble boron by performing an iterative calculation to determine the soluble boron concentration that will maintain the core critical at specified conditions of power level, average inlet moderator temperature, system pressure, control rod positions and the core average burnup.

Comparisons of power distributions, reaction rates and other power distribution related parameters, such as Axial Offset and peaking factors calculated by POLCA and measured at a plant provide an indication of the capability of POLCA to provide reliable power distribution predictions. These comparisons are provided for several cycle exposures for numerous cycles of operation. These comparisons together with the qualification results documented in Reference 1 and in the preceding sections amply demonstrate the capabilities of POLCA and the robustness of its algorithms.

The Plant that was chosen for the comparisons is a Westinghouse built PWR operating in Europe. The core contains 157 fuel assemblies with a 17x17 fuel lattice and rated at 2700 MWth. The reaction rates, measured by the neutron sensitive Traveling Incore Probe (TIP), are shown at several exposure times during a given operating cycle. In addition, assembly average powers, pin powers and core average axial power distributions calculated at the plant using, measured plant parameters, are compared with POLCA calculated values.

5.3.1 POLCA Reactivity Predictions

Comparisons between the measured and calculated critical boron are shown on Figures 5.8 to 5.17, as a measure of the accuracy with which POLCA calculates the core reactivity under normal operating conditions. The critical boron concentration provides a global means of benchmarking the ability of POLCA to calculate the components of the core reactivity due to the fuel depletion, the production of plutonium isotopes, the depletion of burnable poisons, the buildup of fission products, and the local reactivity effects due to changes in moderator temperature and density, the changes in fuel temperature, the effect xenon and samarium and the presence of control rods in the core. The reactivity balance is represented by the change in soluble

boron necessary to maintain the core critical. This global parameter is a good measure of the accuracy of the POLCA solution compared to actual plant operation and differences on the order of [] ppm are considered to indicate very good agreement between calculations and measurement.

There is consistency in the comparisons although there are significant differences in the core loading maps, the length of the operating cycles and the mix of fuel from different vendors, with different burnable poison loading. The observed difference in the measured and calculated soluble boron concentrations varies from as much as [] ppm to as low as [] ppm. The larger observed differences are from cycles of operation of a dozen years ago. The more typical differences in recent cycles are [] ppm or less. Additionally, the largest differences are observed for relatively short time spans typically either at the beginning or at the end of the cycles of operation. This suggests that either some of the measurements could have been taken at non-steady state conditions, e.g. during power ascensions or non-equilibrium conditions near BOC or during coastdown operation at EOC. In either case it is plausible to conjecture that either the measurements or the simulation of the POLCA calculations did not accurately reflect the core status. The inability to accurately reconstruct the core operating history can give rise to differences in the soluble boron concentrations that tend to decrease when the plant has been operating at steady state for long periods of time.

The critical boron concentration differences observed in Cycle 6 and Cycle 10 appear to have a [] in addition to differences between calculation and measurements. If a [] is applied to the calculated critical boron concentration, the remaining differences would be consistent with the differences observed in the other measurements.

5.3.2 Axial Offset and Power Peaking Calculations

Core parameters such as Axial Offset (AO) and power peaking factors; the maximum enthalpy rise (F-delta H) and the maximum 3-dimensional peaking factor (Fq) were calculated by POLCA and compared to the corresponding parameters obtained from plant measurements. Plant measurements, in reality, are not direct measurements of the parameters identified above, rather they are the result of calculations performed computer codes that use measured data and approved methodology. The methodology embodied in the computer codes used at the plant satisfies the requirements placed on performing surveillance of the power peaking factors to validate that the core is operating in compliance with the assumptions made in the Safety Analysis with regard to the magnitude of the allowable power peaking factors.

Figures 5.18 to 5.21 show comparisons of the AO for a number of operating cycles and as a function of burnup in each cycle. The AO comparisons are in

very good agreement between calculations and measurements except for a few cases, i.e. for Cycle 6, Cycle 9 and Cycle 13. Except for these cases, the differences are of the order of [] to [] at most.

The comparisons for the power peaking factors show good agreement. Table 5.5 shows the RMS differences for each of the cycles and for the total population of the measurements collected. The RMS differences for all the F-delta H measurements is \pm [] and for Fq is \pm [].

5.3.3 Power Distribution Comparisons

The power distribution comparisons are shown for sets of representative core average axial shapes and for radial distributions of the average assembly powers.

A number of core average axial power distributions are shown in Figure 5.22 through Figure 5.36. The comparisons between measured and calculated shapes are presented for a number of cycles at burnups representing the Beginning of Cycle (BOC), the Middle of Cycle (MOC) and the End of Cycle (EOC). There is good agreement between the measured core average axial shapes and the POLCA calculations.

The most significant discrepancies are shown at EOC of Cycle 6 and at BOC of Cycle 13. These discrepancies are reflected in the poor agreement in the Axial Offset calculated for those cycles. [

].

A comparison of the axial power peak, F_z , shows good agreement between calculations and measurements as shown in Table 5.6. The differences are less than [] except for a few isolated cases, namely at EOC 5, EOC 6, BOC 9 and EOC 11.

The measurements were obtained from the analysis of the TIP System readings that have a very fine resolution (65 measured points). The calculated values from POLCA are from 34 calculated points. The difference in axial detail is likely to account for some differences in the F_z comparisons, especially in cases when F_z occurs at an axial location which is reflected in the measurements, but does not correspond to an explicitly calculated axial location in the POLCA calculations.

A set of comparisons of radial power distributions and reaction rates, shown in Figure 5.37 to Figure 5.81, indicates that the RMS difference between measured and calculated quantities is of the order of [] for a collection of

comparisons at BOC, MOC and EOC of several cycles of operation, namely Cycle 11 through Cycle 15. The set of comparisons was selected to highlight current operating cycle loading, i.e. current low-leakage loading for later cycles, with different burnable poison loading and cycle lengths.

While the RMS Errors indicate good agreement, there are some maximum and minimum differences that are considerably larger. Most notably a [] difference in the reaction rate at BOC of Cycle 11 for one TIP measurement. This large discrepancy is inconsistent with the assembly average power in symmetrically located assembly, which is different by only [].

The pattern of good agreements overall, as exemplified by the RMS Error and the occasional larger discrepancy in individual measurements, may be partly attributable to the different methods used to generate the cross-sections and calculate the reaction rates and the power distributions, in the measurements and the POLCA calculations. Some of the large discrepancies are also observed in peripheral fuel assemblies indicating that a different reflector treatment may have had an impact on the comparisons.

The comparisons lead to the following conclusions:

- 1) the RMS on the assembly average powers is [] for 2355 measurements.
- 2) the RMS on the maximum pin powers is [] for 2355 measurements.
- 3) the RMS on the reaction rates from the TIP measurements is [] for 684 measurements.

Table 5.7 summarizes the results of the power distribution comparisons.

Table 5.1: Intra-Nodal Depletion Benchmark Results (Cycle 1)

Table 5.2: Intra-Nodal Depletion Benchmark Results (Cycle 2)

Table 5.3: Intra-Nodal Depletion Benchmark Control Rod Worth (RW)

Table 5.4: Summary of Results for NEACRP-L336 Benchmark

Table 5.5: Summary of Results for F-delta H and Fq Comparisons



Table 5.6: Summary of Results for F_z Comparisons

Table 5.7: Summary of Results for Power Distribution Comparisons

Figure 5.1: IAEA 2D Benchmark, POLCA vs. ANL-7416

Figure 5.2: BIBLIS 2D Benchmark, POLCA vs. LABAN

Figure 5.3: DVP Benchmark, POLCA vs PDQ

POWER DISTRIBUTION DIFFERENCES AT BOC1, NO XENON

Figure 5.4: Intra-Nodal Depletion Benchmark, Power Distribution BOC1

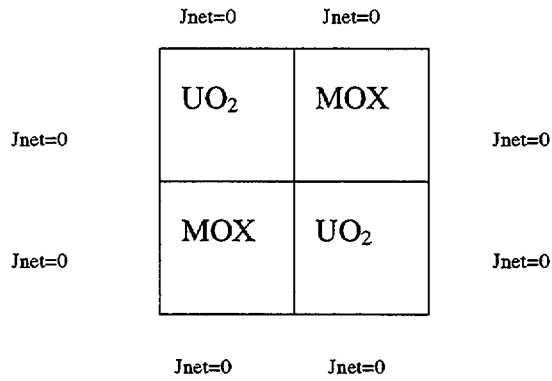


Figure 5.5: UO₂/MOX Checkerboard for NEACRP-L336 Benchmark

Figure 5.6: NEACRP-L336 Benchmark Power Comparison (UO₂ Assembly)

Figure 5.7: NEACRP-L336 Benchmark Power Comparison (MOX Assembly)



Figure 5.8 – Critical Boron Concentration Cycle 6

Figure 5.9 – Critical Boron Concentration Cycle 7

Figure 5.10 – Critical Boron Concentration Cycle 8

Figure 5.11 – Critical Boron Concentration Cycle 9

Figure 5.12 – Critical Boron Concentration Cycle 10

Figure 5.13 – Critical Boron Concentration Cycle 11

Figure 5.14 – Critical Boron Concentration Cycle 12

Figure 5.15 – Critical Boron Concentration Cycle 13

Figure 5.196 – Critical Boron Concentration Cycle 14

Figure 5.17 – Critical Boron Concentration Cycle 15

Cycle 5

Cycle 6

Cycle 7

Figure 5.18 – Axial Offset

Cycle 8

Cycle 9

Cycle 10

Figure 5.19 – Axial Offset

Cycle 11

Cycle 12

Cycle 13

Figure 5.20 – Axial Offset

Cycle 14

Cycle 15

Figure 5.21 – Axial Offset

Figure 5.22 – Cycle 1 Core Average Axial Power Distributions



Figure 5.23 – Cycle 2 Core Average Axial Power Distributions

Figure 5.24 – Cycle 3 Core Average Axial Power Distributions

Figure 5.25 – Cycle 4 Core Average Axial Power Distributions

Figure 5.26 – Cycle 5 Core Average Axial Power Distributions

Figure 5.27 – Cycle 6 Core Average Axial Power Distributions

Figure 5.28 – Cycle 7 Core Average Axial Power Distributions



Figure 5.29 – Cycle 8 Core Average Axial Power Distributions

Figure 5.30 – Cycle 9 Core Average Axial Power Distributions

Figure 5.31 – Cycle 10 Core Average Axial Power Distributions

Figure 5.32 – Cycle 11 Core Average Axial Power Distributions

Figure 5.33 – Cycle 12 Core Average Axial Power Distributions

Figure 5.34 – Cycle 13 Core Average Axial Power Distributions

Figure 5.35 – Cycle 14 Core Average Axial Power Distributions

Figure 5.36 – Cycle 15 Core Average Axial Power Distributions



Figure 5.37 – Cycle 11 BOC

Figure 5.38 – Cycle 11 BOC

Figure 5.39 – Cycle 11 BOC

Figure 5.40 – Cycle 11 MOC



Figure 5.41 – Cycle 11 MOC

Figure 5.42 – Cycle 11 MOC

Figure 5.43 – Cycle 11 EOC



Figure 5.44 – Cycle 11 EOC

Figure 5.45 – Cycle 11 EOC

Figure 5.46 – Cycle 12 BOC

Figure 5.47 – Cycle 12 BOC

Figure 5.48 – Cycle 12 BOC



Figure 5.49 – Cycle 12 MOC

Figure 5.50 – Cycle 12 MOC



Figure 5.51 – Cycle 12 MOC

Figure 5.52 – Cycle 12 EOC

Figure 5.53 – Cycle 12 EOC

Figure 5.54 – Cycle 12 EOC

Figure 5.55 – Cycle 13 BOC



Figure 5.56 – Cycle 13 BOC

Figure 5.57 – Cycle 13 BOC

Figure 5.58 – Cycle 13 MOC

Figure 5.59 – Cycle 13 MOC

Figure 5.60 – Cycle 13 MOC



Figure 5.61 – Cycle 13 EOC

Figure 5.62 – Cycle 13 EOC



Figure 5.63 – Cycle 13 EOC

Figure 5.64 – Cycle 14 BOC

Figure 5.65 – Cycle 14 BOC

Figure 5.66 – Cycle 14 BOC

Figure 5.67 – Cycle 14 MOC

Figure 5.68 – Cycle 14 MOC



Figure 5.69 – Cycle 14 MOC

Figure 5.70 – Cycle 14 EOC



Figure 5.71 – Cycle 14 EOC

Figure 5.72 – Cycle 14 EOC

Figure 5.73 – Cycle 15 BOC

Figure 5.74 – Cycle 15 BOC

Figure 5.75 – Cycle 15 BOC



Figure 5.76 – Cycle 15 MOC

Figure 5.77 – Cycle 15 MOC

Figure 5.78 – Cycle 15 MOC



Figure 5.79 – Cycle 15 EOC

Figure 5.80 – Cycle 15 EOC

Figure 5.81 – Cycle 15 EOC

6.0 SUMMARY

The PHOENIX/POLCA code system has been used for the analysis of Nordic reactors since the late 1960's and has been used in the United States since the mid 1980's. In addition, the POLCA 3D core simulator has been used for on-line core monitoring in Nordic plants since 1974.

The PHOENIX/POLCA code system described in this topical report is an application to Pressurized Water Reactors of the system discussed in Reference 1.

The PHOENIX/POLCA code system with the ENDFB-VI cross section library has been tested by comparison with higher order analytical solutions and experimental data. Code predictions have been compared with critical facility measurements as well as operating plant data. This section summarizes results and conclusions based on the qualification relative to measurements discussed in Sections 3 and 5 as well as overall conclusions.

6.1 PHOENIX BENCHMARKS TO TEST THE ENDFB-VI LIBRARY

The calculational models, approximations and methods in the PHOENIX code are the same as those described in Reference 1. Qualification results with the 34-group cross section library are provided in Section 3 as an illustration of the ABB methodology for qualifying a cross section library. PHOENIX, and the associated nuclear data pre- and post-processing codes, has been modified only to the extent required to support the new cross section library and the POLCA improvements as described in Reference 1.

Since the primary application of PHOENIX is to generate the few-group nodal cross sections and other physics constants for POLCA, the best overall qualification of PHOENIX and the new library is the comparison of POLCA predictions with experimental data described in Chapter 5. However, comparison of PHOENIX predictions with measured data allows the capability of PHOENIX, in conjunction with the 34-group cross section library, to be evaluated independent of approximations involved in the POLCA methods and the additional experimental uncertainties involved with operating plant measurements.

The comparisons with the Strawbridge and Barry and BAPL uniform lattice critical measurements confirmed the capability of PHOENIX to accurately calculate reactivity over a wide range of lattice parameters. Because of the simple geometry in those experiments, the comparisons primarily provided verification and validation of the new cross section library.

In addition, the ability of PHOENIX to accurately predict bundle reactivity and internal (local) power distributions was verified by comparison with

experimental results obtained for nonuniform UO₂ and PuO₂ lattices performed at the KRITZ critical facility.

As shown in Table 3.10, the mean $k_{\text{effective}}$ for the UO₂ Strawbridge and Barry criticals, the BAPL criticals, and the UO₂ and PuO₂ KRITZ experiments is [] with a total spread in the average $k_{\text{effective}}$ values for each of the four experimental sets of []. The proximity to unity and the relatively small spread in these average values demonstrate excellent agreement with the experimental data.

Furthermore, the PHOENIX predictions showed very good agreement with the KRITZ pin power (i.e. fission rate) measurements. The mean absolute differences in predicted and measured pin powers were [] for the UO₂ and PuO₂ KRITZ experiments, respectively, with corresponding maximum differences of [].

The combination of these results confirm that PHOENIX, in conjunction with the new ENDF/B-VI based 34-group library, provides state-of-the-art reactivity and relative pin power predictions for a broad range of conditions and temperatures.

6.2 POLCA QUALIFICATION

The qualification of POLCA in Section 5 is divided into two categories, referred to as verification and validation. In the context of this report, verification involves the testing of individual models or combinations of models to verify that they perform as intended. Validation involves the comparison of POLCA predictions with measured data to establish the accuracy of the system operating as a whole. The POLCA verification was performed by comparison with computational benchmarks generated by means of reference calculations as well as by comparison with experimental data suitable for evaluating the individual model being verified.

6.2.1 Reactivity

ABB performs POLCA core follow calculations for plants for which it has nuclear design responsibility or in the continuing process of validating its nuclear design codes. The core reactivity behavior is exemplified by the critical boron concentration that is maintained at operating plants during power operation.

The critical boron concentration measured in a PWR during several operating cycles is discussed in Section 5.3.1. The predictability of the critical boron is demonstrated by the good agreement between measurements and calculations, which is within [] ppm for most of the comparisons carried out. The [] ppm value corresponds approximately to a [] pcm difference. Some larger

differences have been observed and discussed in Section 5.3.1 and can be attributed to inconsistencies in the comparisons that can be due to calculations being performed at non-steady state conditions, e.g. during the early parts of an operating cycle when the effects of non-equilibrium xenon and samarium concentrations could not accurately be captured in the core follow data. The overall agreement leads to the conclusion that the PHOENIX/POLCA code system with the new cross section library provides sufficiently stable and predictable reactivity behavior that includes the effects of fuel burnup, burnable poisons depletion and local reactivity feedbacks.

6.2.2 Power Distributions

The capability of POLCA to predict core parameters such as the Axial Offset and power peaking factors was evaluated for a number of operating cycles and discussed in Section 5.3.2.

The Axial Offset comparisons show good agreement between measurement and calculations, with differences except in the few cases identified in Section 5.3.2 of less than [].

The comparison of the power peaking factors shows that the RMS differences for $F_{\text{delta H}}$ and for F_q are $\pm[]$ and $\pm[]$ respectively. The differences provide an indication of the power peaking uncertainties associated with POLCA.

6.2.3 Power Distribution Comparisons

The capability of POLCA to predict power distributions, pin power peaks and reaction rates for in-core detector measurements was carried out for a number of operating cycles and discussed in Section 5.3.3 at several times during the operation of a given cycle.

The conclusions that can be reached from the comparisons are as follows:

1. the RMS on the assembly average powers is []
2. the RMS on the maximum pin powers is []
3. the RMS on the reaction rates from TIP measurements is []

The POLCA predictions provide an indication of the fuel assembly average power, maximum pin power and reaction rates uncertainties associated with POLCA.

These estimated uncertainties confirm that the POLCA capability for predicting power distributions and peaking factors is sufficient for the analysis of relevant PWR reactor configurations under steady-state conditions.

6.3 OVERALL CONCLUSION

The qualifications of the PHOENIX/POLCA code system are based on comparisons with higher order calculations, measurements from operating plants, and experimental results from critical configurations. These comparisons demonstrate that the methodology is capable of satisfactory analysis of relevant PWR reactor configurations and steady-state operating conditions.

Therefore, it is concluded that the qualification process has demonstrated the PHOENIX/POLCA capability analysis of relevant PWR reactor configurations under steady-state conditions. The PHOENIX/POLCA system provides state-of-the-art results acceptable for design and licensing applications.

7.0 REFERENCES

1. The Advanced PHOENIX and POLCA Codes for Nuclear Design of Boiling Water Reactors, CENPD-390-P (proprietary), CENPD-390-NP (nonproprietary), April 1999 (under NRC review)
2. A Description of the Nuclear Design and Analysis Programs for Boiling Water Reactors, Westinghouse Report WCAP-10106-P-A (proprietary), WCAP-10999-NP-A (nonproprietary), September 1985.
3. Qualification of the PHOENIX/POLCA Nuclear Design and Analysis Programs for Boiling Water Reactors, Westinghouse Report WCAP-10841-P-A (proprietary), WCAP-10842-NP-A (nonproprietary), June 1985.
4. Letter from C. O. Thomas (NRC) to E. P. Rahe (W), "Acceptance for Referencing of Licensing Topical Report WCAP-10106, 'A Description of the Nuclear Design and Analysis Programs for Boiling Water Reactors'," September 3, 1985.
5. Letter from M. W. Hodges (NRC) to W. J. Johnson (W), "Acceptance for Referencing of Licensing Topical Report WCAP-10841, 'Qualification of the PHOENIX/POLCA Nuclear Design and Analysis Programs for Boiling Water Reactors'," June 14, 1988.
6. Letter from A. L. Thadani (NRC) to J. Lindner (ABB Atom), "Designation of ABB Atom Topical Reports Related to Licensing of ABB Atom Reload Fuel," June 18, 1992.
7. Letter from G. Heimersson (ABB Atom) and A. E. Scherer (ABB CE) to R. C. Jones, Jr. (NRC), "ABB BWR Fuel and Core Component Licensing Activities," September 4, 1992.
8. R. R. Lee et al., "The Benchmark Problem Book," Argonne Code Centre, Report ANL-7416, Supplement 2, 1977.
9. E. Z. Muller and Z. J. Weiss, "Benchmarking with the Multigroup Diffusion High-Order Response Matrix Method," *Annals of Nuclear Energy*, Vol. 18, No. 9, p. 534, 1991.
10. K. S. Smith, "Assembly Homogenization Techniques for Light Water Reactor Analysis," *Progress in Nuclear Energy*, Vol. 17, No. 3, pp. 303-335, 1986.
11. E. Z. Muller et al., "Development of a Core Follow Computational System for Research Reactors," Ninth Pacific Basin Nuclear Conference, Sydney, Australia, May 1994.
12. K. Koebke et al., "The Benchmark Problem Book," Argonne Code Centre, Report ANL-7416, Supplement 3, 1985.
13. J. Lefvebre, J. Mondot and J. P. West, "Benchmark Calculations of Power Distribution Within Assemblies (Specification)," NEACRP-L-336, 1991.